Interactions of iron implants in transition metals

J. Stanek
Institute of Physics, Jagiellonian University, Reymonta 4, 30-059 Cracow, Poland

G. Marest and H. Jaffrezic
Institut de Physique Nucleaire de Lyon, Institute National de Physique Nucléaire et de Physique des Particules, Centre National de la Recherche Scientifique et Universite Claude Bernard, 43, Boulevard du 11 Novembre 1918, 69622 Villeurbanne Cedex, France

H. Binczycka
Institute of Physics, Jagiellonian University, Reymonta 4, 30-059 Cracow, Poland
(Received 13 March 1995)

Au, Ir, Pt, Rh, Ti, and W foils were implanted with ^{57}Fe ions with doses from 10^{15} to 5×10^{16} ions/cm^2 and studied at room temperature by conversion electron Mössbauer spectroscopy. It has been proved that the macroscopic heat of solution of Fe in respective metals is a primary parameter determining the state of implanted specimens. For an attractive Fe-Fe potential the iron implants are observed in the form of aggregates, while for a repulsive Fe-Fe potential, they are not distinguishable in Mössbauer spectra. Molecular-dynamics simulations showed that the final arrangement of atoms within a thermal spike is maintained during about 1.2 ps.

INTRODUCTION

The macroscopic description of processes of metal alloying is linked with microscopic quantities within the Miedema model.[1] This model delivers the microscopic bonding energies of interacting metal atoms in alloys with the use of the macroscopic heats of formation. The experimental determination of these energies appears interesting for that particular model as well as for any *ab initio* calculations. In fact, there is already a wide documentation based mainly on perturbed angular correlation measurements[2–4] confirming the reliability of the Miedema approach for description of impurity-impurity interaction in diluted ternary systems at thermodynamical equilibrium. It was proved that macroscopic heats of solution of corresponding systems are related to the bonding energy of impurity aggregates.

However, an open question remains: "can the Miedema model be extended for the characterization of metastable systems, for instance, quenched alloys or, as considered in this paper, implanted specimens?" If so, how far? In the early stage of the investigation of iron implants in metals using conversion electron Mössbauer spectroscopy the Miedema concept was employed for a qualitative explanation of the obtained results[5–7] in terms of localization of implants, trend in their aggregation, amorphization of the targets or magnitude of the hyperfine parameters. The later increase in the accuracy of experimental data did not change the situation significantly. The main reason for this is that for the determination of the bonding energies between elements forming a metastable alloy, one must assign to the system an effective equilibrium temperature, that temperature at which the system has been frozen. Such estimates are very doubtful for quenched systems and appeared rather impossible for implanted samples.

Recently, it has been shown[8] that the enhanced aggregation of iron implants in silver may be quantitatively described by using the melting temperature of silver as the equilibrium temperature, i.e., assuming an extremely high cooling rate. Under this assumption, the experimentally determined bonding energy for Fe-Fe dimer is not far from that calculated from Miedema model.[1]

In this work, the results of conversion electron Mössbauer spectroscopy (CEMS) studies on transition metals (Ag, Au, W, Ir, Pt, Rh, Ti) implanted with ^{57}Fe ions are presented. For Ag and Au the attractive Fe-Fe interaction is expected, while for Ir, Pt, Rh, and Ti these interactions should be repulsive. W is an intermediate case with apparently vanishing interaction between iron impurities. With the exception of W (bcc) and Ti (hcp) the investigated targets have a fcc structure type. Similar investigations have been carried out in the past by many authors, see, for example, Refs. 5–7 and 9–15. In particular, the data reported for Cu implanted with ^{57}Fe ions[14] are used here in discussion. It would be rather difficult to review in detail the results of these previous studies. However, one may risk the conclusion that, as a rule, the obtained spectra are complicated and not well resolved. This certainly causes an ambiguity in their interpretation. Quite frequently the data have been described using one of the two extreme approaches: (i) a macroscopic approach, where the spectra have been decomposed into contributions arising from different intermetallic compounds known from binary equilibrium phase diagrams and, (ii) a microscopic approach, which for the implanted samples neglects the metallurgy and deals with isolated Fe impurities and Fe aggregates of rather unknown structure. In both cases, the influence of radiation damage in the samples is frequently used as a comfortable explanation of appearing discrepancies.

0163-1829/95/52(11)/8414(9)/$06.00

TABLE I. Calculated parameters of iron concentration profiles in the studied samples. R_p and R_{max} are the mean and maximum ranges, ΔR_p is the standard deviation of R_p, C_{max} is the iron atomic concentration at the maximum of the ion distribution, and C_{av} is the iron average concentration in the implanted zone.

Host	Energy (keV)	Fluence (10^{15} ions/cm^2)	Dose (10^{15} ions/cm^2)	R_p (nm)	ΔR_p (nm)	R_{max} (nm)	C_{max} (%)	C_{av} (%)
Au	100	1	0.88	28.0	16.6	80	0.36	0.22
	100	2	1.73	27.5	16.1	80	0.79	0.48
	100	5	4.35	28.2	16.6	80	1.69	1.02
	100	10	8.7	28.0	16.0	80	3.40	2.06
	100	20	17.4	24.6	14.6	80	7.48	4.54
Pt	100	10	8.80	28.0	16.4	75	3.64	2.21
	100	30	26.4	27.8	16.3	80	10.3	6.25
	100	50	44.3	28.3	16.2	80	16.0	9.70
Rh	70	5	4.81	20.6	11.7	60	2.2	1.33
	70	10	9.60	21.1	11.8	60	4.3	2.61
	70	20	19.3	21.0	11.8	60	8.8	5.34
Ti	70	5	5.00	39.8	18.2	100	1.9	1.15
	70	10	10.0	39.1	17.9	100	3.8	2.30
	70	20	20.0	39.7	18.2	90	7.2	4.37
W	100	5	4.4	25.9	15.1	80	1.85	1.12
	100	10	8.9	25.4	14.8	80	3.9	2.37
	100	20	17.8	25.6	14.9	80	7.2	4.37
Ir	100	5	4.3	23.0	14.0	70	1.75	1.06

EXPERIMENT

Au, Ir, Pt, Rh, W, and Ti foils were implanted at room temperature with 100 or 70 keV ^{57}Fe ions. The fluence (i.e., implanted dose) varied from 10^{15} to 5×10^{16} ions/cm^2. The remaining doses and the parameters of iron concentration profiles in all studied samples, collected in Table I, were calculated using TRIM program.[16]

The ^{57}Fe CEMS spectra of implanted samples were recorded at room temperature with a He-5% CH_4 gas-flow proportional counter. The ^{57}Co/Rh source of the activity of 50 mCi was used. Some samples were studied after subsequent (10 min) annealings under flowing hydrogen gas in the temperature range 200–500 °C.

The spectra were evaluated using the Lorentzian lines fit approximation. In the case studied, no disturbance of the resonant line shape due to finite absorber thickness is expected in our scattered spectra, which is a serious problem for transmission technique. However, in implanted samples the distribution of hyperfine parameters is quite common. This certainly causes broadening of absorption lines and alters their shape. Thus, in some cases such distributions, mainly of quadrupole splitting (QS) distribution, were considered and evaluated by the use of the program developed by Le Caer and Dubois.[17] The isomer shift (IS) is given vs metallic iron.

RESULTS

CEMS spectra corresponding to Au implanted with various ion fluences are displayed in Fig. 1. The fitted hyperfine parameters are given in Table II. The Mössbauer spectra of ^{57}Fe implanted in Au with the low doses consist of one single line, which IS corresponds to isolated Fe ions in gold,[11] and of one quadrupole doublet with the IS shifted towards metallic iron shift. This doublet assigned to iron dimers[18] has a relative population

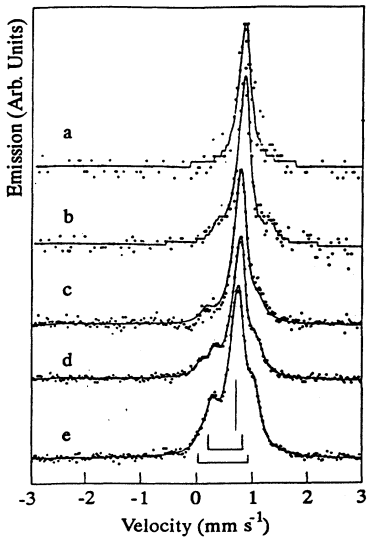

FIG. 1. Room-temperature ^{57}Fe CEMS spectra of iron implanted in Au with the fluences of 10^{15} (a), 2×10^{15} (b), 5×10^{15} (c), 10^{16} (d), 2×10^{16} ions/cm^2 (e). The implantation energy was 100 keV. The positions of the lines are indicated.

TABLE II. Hyperfine parameters of ^{57}Fe implanted into transition metals. IS = isomer shift vs metallic iron, QS = quadrupole splitting, W = linewidth, f = fraction of each component.

			Fe in Au					
Fluence (10^{15} ions/cm^2)	1	2	5	10	20	20	20	
Annealing (°C)						200	300	
IS (mm/s)	0.64	0.66	0.64	0.65	0.64	0.64	0.64	monomer
QS (mm/s)						0.10		
W (mm/s)	0.26	0.24	0.26	0.26	0.25	0.25	0.22	
f (%)	89	86	89	74	62	66	38	
IS (mm/s)	0.54	0.70	0.54	0.58	0.59	0.60	0.49	dimer
QS (mm/s)	0.88	0.84	0.88	0.68	0.68	0.73	0.78	
W (mm/s)	0.23	0.22	0.22	0.22	0.29	0.22	0.50	
f (%)	11	14	11	17	27	17	51	
IS (mm/s)				0.52	0.55	0.48		trimer
QS (mm/s)				1.00	0.92	0.76		
W (mm/s)				0.22	0.29	0.33		
f (%)				9	11	17		
IS (mm/s)							−0.01	aggregates
QS (mm/s)							0.77	
W (mm/s)							0.67	
f (%)							11	
			Fe in Pt					
Fluence (10^{15} ions/cm^2)	10	30	30	30	30	50		
Annealing (°C)			200	300	500			
IS (mm/s)	0.34	0.33	0.34	0.34	0.35	0.33		monomer
QS (mm/s)	0.13	0.13	0.13	0.13	0.09	0.13		
W (mm/s)	0.22	0.22	0.22	0.22	0.22	0.22		
f (%)	93	94	91	91	97	93		
IS (mm/s)	0.34	0.33	0.34	0.34	0.35	0.33		monomer-
QS (mm/s)	0.47	0.44	0.50	0.49	0.57	0.55		defect
W (mm/s)	0.22	0.22	0.22	0.22	0.22	0.22		complex
f (%)	6	6	9	7	3	6		
			Fe in Ir					
Fluence (10^{15} ions/cm^2)	5							
IS (mm/s)	0.26							monomer
W (mm/s)	0.30							monomer
f(%)	100							
			Fe in Rh					
Fluence (10^{15} ions/cm^2)	5	10	10*	10*	10*	20		
Annealing (°C)				400	500			
IS (mm/s)	0.09	0.11	0.11	0.10	0.10	0.08		monomer
W (mm/s)	0.36	0.37	0.41	0.31	0.31	0.41		
f (%)	39	46	36	77	95	41		
IS (mm/s)	0.10	0.11	0.08			0.18		monomer+
QS (mm/s)	0.68	1.03	0.73			0.54		defect (1)
W (mm/s)	0.40	0.25	0.33			0.40		
f (%)	26	5	13			32		
IS (mm/s)	0.44	0.33	0.37			0.29		monomer+
QS (mm/s)	0.80	1.05	0.96			1.05		defect (2)
W (mm/s)	0.30	0.31	0.45			0.26		
f (%)	6	12	24			5		
IS (mm/s)	0.66	0.51	0.58	0.46	0.47	0.63		monomer+
QS (mm/s)	0.83	1.14	1.05	0.88	0.99	0.80		defect (3)
W (mm/s)	0.58	0.56	0.51	0.53	0.22	0.47		
f (%)	29	37	31	22	5	16		

TABLE II. (*Continued*).

	Fe in Ti			
Dose (10^{15})	5	10	20	
IS (mm/s)	0.02	0.00	0.00	monomer
W (mm/s)	0.30	0.24	0.20	α-Ti(Fe)
f (%)	17	12	7	
IS (mm/s)	−0.18	−0.16	−0.15	monomer
QS (mm/s)	0.48	0.44	0.39	β-Ti(Fe)
W (mm/s)	0.58	0.51	0.46	
f (%)	70	80	80	
IS (mm/s)	0.66	0.74	0.60	Fe oxides
W (mm/s)	0.68	0.88	0.97	
f (%)	13	8	13	

which increases with iron concentration up to 27% for the fluence of 2×10^{16} ions/cm^2. For higher doses, starting from 10^{16} ions/cm^2, a second doublet with still a lower IS is observed. This doublet is assigned to iron trimers.[18] Although the spectra of Au implanted with ^{57}Fe ions are quite similar to those of ^{57}Fe implanted Ag, reported elsewhere[8] or in Cu,[10–14] their comparison indicates a significant difference in the respective ratios of doublets to singlet areas.

Annealing experiments were performed on the sample implanted with 2×10^{16} ions/cm^2. After annealing at 200 °C the fraction of trimers increases at the expense of iron monomers, while the fraction of dimer remains unchanged. At 300 °C, the intensity of the monomer line strongly decreases (down to 38%) and the dimer fraction becomes dominant (51%). At the same time the trimers disappear, being replaced by superparamagnetic iron clusters with IS of 0 mm/s (see Fig. 2 and cf. Table II).

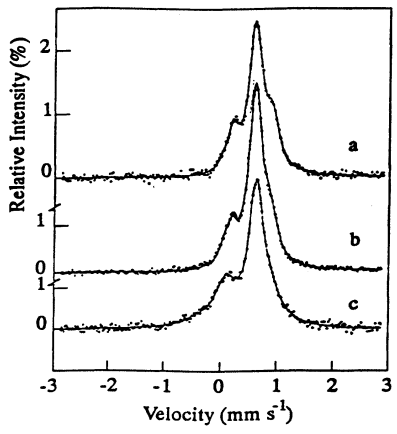

FIG. 2. Room-temperature ^{57}Fe CEMS spectra of iron implanted in Au with the fluence of 2×10^{16} ions/cm^2 and the energy of 100 keV after subsequent 10 min annealing under flowing hydrogen gas at temperatures 200 °C (b), 300 °C (c). The spectrum of unannealed sample (a) is shown for comparison.

Similar thermal evolution has been observed for Ag implanted with Fe,[8] with the difference that in that case the fraction of monomers decreased already at 200 °C and the dimers were converted into small superparamagnetic iron particles at 300 °C. The Mössbauer spectrum of ^{57}Fe implanted in Ir at the fluence of 5×10^{15} ions/cm^2 consists exclusively of a Lorentzian shape single line with the IS of diluted iron impurities in this matrix (IS = 0.26 mm/s).[11]

The CEMS spectra of ^{57}Fe implanted in Pt are shown in Fig. 3. The apparently symmetric single lines with IS=0.34 mm/s could not be reproduced by a single Lorentzian line fit. Thus, the spectra were fitted assuming a distribution of the QS with the same IS for all com-

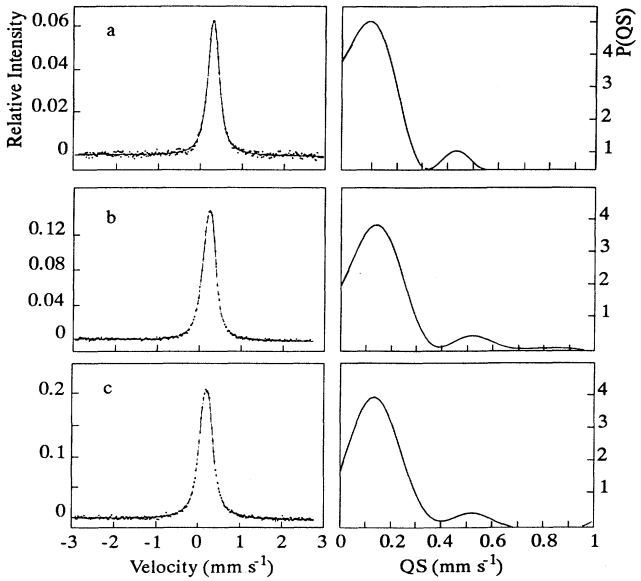

FIG. 3. Room-temperature ^{57}Fe CEMS spectra of iron implanted in Pt with the fluences of 10^{16} (a), 3×10^{16} (b), 5×10^{16} ions/cm^2 (c), (left) and corresponding distribution of quadrupole splittings, QS, (right). The implantation energy was 100 keV.

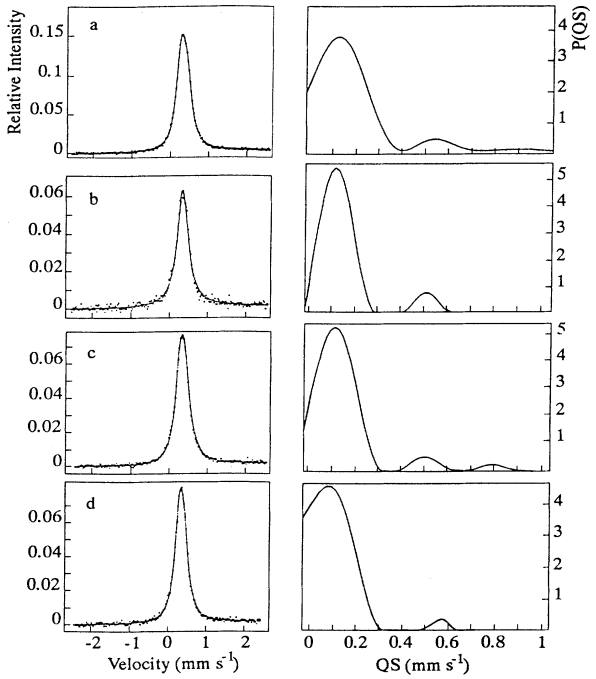

FIG. 4. Room-temperature ^{57}Fe CEMS spectra of iron implanted in Pt with the fluence of 3×10^{16} ions/cm^2 (left) and corresponding distribution of quadrupole splittings, QS, (right) after annealing at temperatures 200 °C (b), 300 °C (c), 500 °C (d). The spectrum of unannealed sample (a) is shown for comparison. The implantation energy was 100 keV.

ponents. The obtained distributions are shown in Fig. 3 as well. In as-implanted samples, with the exception of the substitutional fraction, an additional component with an average QS increasing from 0.47 mm/s for the fluence of 10^{16} ions/cm^2 to 0.55 mm/s for the fluence of 5×10^{16} ions/cm^2 is clearly seen. The intensity of this fraction (7%) is nearly dose independent. The thermal evolution of this component was studied by annealing the sample implanted with the fluence of 3×10^{16} ions/cm^2. The obtained spectra and corresponding QS distributions are shown in Fig. 4. Already after 200 °C annealing, the QS distribution becomes sharper. Its maximum located at 0.5 mm/s splits after annealing at 300°C into two peaks located around 0.5 and 0.8 mm/s, and nearly disappears after annealing at 500 °C. In Table II the average QS, obtained from the distribution curves, are given.

The Mössbauer spectra of ^{57}Fe implanted in Rh with fluences of 5×10^{15}, 10^{16}, and 2×10^{16} ions/cm^2 are shown in Fig. 5. The corresponding hyperfine parameters are collected in Table II. The main component in the spectrum is one single line with IS=0.10 mm/s assigned to substituted iron in Rh lattice.[11] This single line is overlapped by a second component, a quadrupole doublet, having the same IS as the single line. In addition, two quadrupole doublets with larger IS are visible in the spectra. The iron states corresponding to these doublets are rather unstable as they disappear nearly completely after

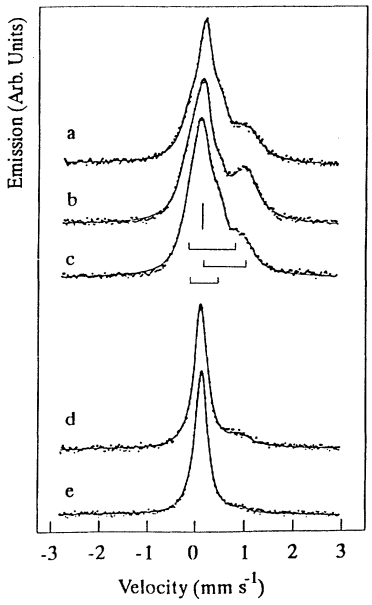

FIG. 5. Room-temperature ^{57}Fe CEMS spectra of iron implanted in Rh with the fluences of 5×10^{15} (a), 10^{16} (b), 2×10^{16} ions/cm^2 (c), and of the sample implanted with 10^{16} ions/cm^2 annealed at temperature 400 °C (d) and 500 °C (e). The implantation energy was 70 keV. The positions of the lines are indicated.

annealing at 500 °C as shown in Fig. 5(e).

All the metals implanted with ^{57}Fe discussed so far were of fcc structure. Ti is the only metal with hcp structure studied in this work. The CEMS spectra, shown in Fig. 6, are composed of three components with parameters given in Table II. The IS of the dominating quadrupole doublet agrees with the value given for bcc β-Ti(Fe) phase obtained for samples produced by vapor quenching[19] or by quenching alloyed specimens.[20] Thus, that fraction may be ascribed to the β-Ti(Fe) bcc phase in spite of the fact that the QS is by 0.2 mm/s larger than reported in the literature.[19,20] This discrepancy could be

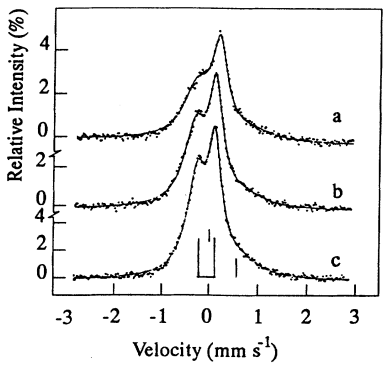

FIG. 6. Room-temperature ^{57}Fe CEMS spectra of iron implanted in Ti with the fluences of 5×10^{15} (a), 10^{16} (b), 2×10^{16} ions/cm^2 (c). The implantation energy was 70 keV. The positions of the lines are indicated.

explained by more distorted structures in our implanted sample than in the classically quenched specimens. An alternative assignment of the discussed fraction might be iron located in tetrahedral interstitial site.[13] The weak single line in the spectrum with IS=0 mm/s is attributed to α-Ti(Fe) hcp phase. The last fraction, characterized by a weak broad line with a large IS of about 0.65 mm/s is probably due to some oxidation of Fe ions during the implantation process.

W (bcc structure) was implanted with ^{57}Fe with three fluences: 5×10^{15}, 10^{16}, and 2×10^{16} ions/cm^2. For the lowest dose studied, the spectrum consists of a single line and of two quadrupole doublets with splittings of 0.70 and 2.38 mm/s and isomer shifts of 0.32 and 0.99 mm/s, respectively. For the intermediate dose of 10^{16} ions/cm^2, the doublet with the smaller splitting vanishes, but becomes the only component for the sample implanted with 2×10^{16} ions/cm^2. Without ambiguity these two doublets are due to Fe^{3+} and Fe^{2+} species. Thus, we have excluded these samples from further discussion as they do not display the expected monomer or dimer components.

DISCUSSION

The initial random distribution of implanted ions undergoes a relaxation during the thermal spike until being frozen at a temperature, T, which prohibits the further migration of adatoms. As a result, the number of isolated impurities (monomers) and of their aggregates of i atoms varies with the time to minimalize the free energy. We have simulated this process by the molecular-dynamics method[21] at 1200 K. As an example the Ag sample implanted with 2×10^{16} Fe ions/cm^2 of energy 100-keV was chosen. The average atomic concentration of implanted iron, in that case, was 4.5%.

At first the silver fcc lattice at 300 K with $7^3\times4=1372$ atoms was constructed. Next, 61-Ag atoms (4.5%) were randomly replaced by Fe atoms. Within the tight-binding model,[22] the cohesive energy of each atom k may be written in the form of the sum of a two-body repulsive energy, $E^k_{\rm rep}$,

$$E^k_{\rm rep}=\sum_{i,j} A_{ij}\exp\left[-p_{ij}\left[\frac{d_{ij}}{d_{oij}}-1\right]\right], \quad (1)$$

and attractive band energy, E^k_b,

$$E^k_b=-\left\{\sum_{i,j}\xi^2_{ij}\exp\left[-2q_{ij}\left[\frac{d_{ij}}{d_{oij}}-1\right]\right]\right\}^{1/2}, \quad (2)$$

where d_{ij} is the distance between atoms i and j, d_{0ij} is the corresponding first-neighbor distance. The parameters A_{ij}, ξ_{ij}, p_{ij}, and q_{ij} were taken from[23] as determined by fitting experimental cohesive energy, lattice parameter, and elastic constants with the modification of d_0, Ag-Ag nearest-neighbor distance, to obtain ambient pressure at 1200 K. For Fe-Fe interactions, the four parameters were determined by fitting the cohesive energy and lattice parameter of γ-Fe (fcc). Finally, for the Fe-Ag potential, the related parameters were assumed as the average of those used for Ag-Ag and Fe-Fe potentials. The used parameters are

	A(eV)	ξ(eV)	p	q	d_0(Å)
Ag-Ag	0.099 82	1.1663	10.84	3.05	2.885
Fe-Fe	0.133 15	1.6179	10.50	2.60	2.553
Fe-Ag	0.116 485	1.3921	10.67	2.825	2.553

Certainly, this description of the Fe-Fe and Fe-Ag interactions in Ag lattice is very crude. However, it was proved that their modification does not significantly influence the time evolution of the system, which is of our primary interest.

Next, the influence of the increase in temperature from 300 K up to 1200 K, i.e., just below the Ag melting temperature, was simulated using the method described in Ref. 24. Finally, the relaxation of the system at the constrained temperature of 1200 K was followed, using the Verlet method[25] for integrating the equation of motion in time steps $dt=10^{-15}$ s. This relaxation was analyzed in terms of numbers of iron monomers, dimers, trimers, etc., i.e., the quantities which are experimentally observable. It turns out that the system stabilizes in the quite short time of 1.2 ps, which is concluded from the stabilization of the total energy and from the steady population in time of the different iron species. The evolution of the cluster distribution as a function of the time is displayed in Fig. 7.

The performed simulations reproduce the strong tendency for iron atoms precipitation in Ag during the

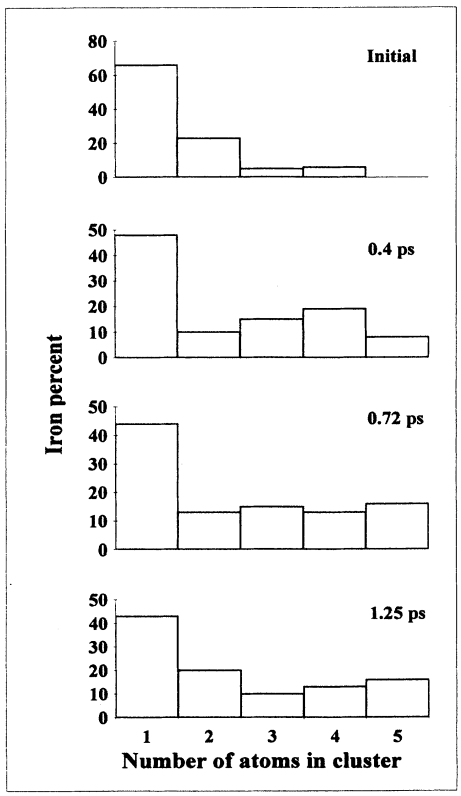

FIG. 7. Results of the molecular-dynamics calculations for a 4.5% atomic concentration of Fe in Ag. Distribution of iron species in Ag at 1200 K after 0, 0.4, 0.72, 1.25 ps.

thermal spike, but the monomer fraction (43%) and the dimer fraction (29%) are, respectively, significantly higher and lower than those observed experimentally, i.e., 24% for monomers and 34% for dimers. The Fe-Fe distance in dimeric state, 2.4 Å, is shorter than Ag-Ag nearest distance in the host (2.885 Å). Thus, the iron dimers are expected to be in the form of dumbbell-like molecules immersed in the host. The energy of the iron monomer is -2.65 eV, while the energy of the iron atom in dimers is -2.80 eV. Thus, the formation of an iron dimer lowers the energy of the system by 300 meV.

Consequently, the original aim of this work was an attempt to describe the localization and interaction between iron implants in transition metals using only one parameter, i.e., the potential of Fe-Fe bonding obtained from the Miedema model. The microscopic binding energy of a homoatomic dimer compared with the energy of i monomers, E_2^*, in a diluted alloy is related to the macroscopic heat of solution, H, as $E_2^* = -2H/Z$, where Z is the coordination number of the related host. The discussion presented below is separated for two cases: hosts with expected (i) attractive Fe-Fe potential (Ag, Au, Cu) and, (ii) repulsive potential (Ir, Pt, Rh, and Ti).

(i) State of iron implants in Ag, Au, and Cu. For matrices in which an attractive potential between Fe-Fe impurities can be assumed on the basis of the Miedema model of alloying, the discussion of the results will be based on the consideration of the probability of formation of different iron aggregates, as presented in Ref. 8 for iron implanted in Ag. The free energy F of the system consisting of the iron impurity molecules is

$$F=\sum_{i=1} E_i n_i - T \sum_{i=1} S_i \ , \tag{3}$$

where E_i is the bonding energy of an iron molecule, n_i is the number of the iron molecules, S_i is the configuration entropy, $S_i = k\ln\Omega_i$, where Ω_i is the number of ways in which n_i aggregates of i identical atoms may be distributed over N lattice sites:

$$\Omega_i = \frac{(k_i N)!}{(k_i N - n_i)! n_i!} \ , \tag{4}$$

where $k_i = \binom{Z}{i-1}/i$. Finally, the energy of an iron molecule, E_i^*, compared with the energy of i monomers, $E_i^* = E_i - iE_1$ is

$$E_i^* = -kT \ln \left[\frac{f_i}{k_i f_1^i c^{i-1}} \right] \ , \tag{5}$$

where T is the equilibrium temperature, here arbitrarily assumed as being the melting temperature, c is the average atomic concentration and f_i is the relative population of iron impurity in aggregates of i atoms. The equation (5) is valid only in the low concentration limit. For a random distribution of impurity atoms, when f_i is given by the binomial distribution, which means $E_i^* = 0$, Eq. (5) gives

$$E_i^* = -kT \ln(1-c)^{-(i-1)(Z+1)} \to 0 \text{ if } c \to 0 \ . \tag{6}$$

For Fe dimers in Ag, $E_2^* = -240$ meV was obtained. This disagrees with the values concluded from the Miedema model (-178 meV) and from molecular-dynamics calculations (-300 meV). This discrepancy is qualitatively explained as follows. Within the simplification of the Miedema model, the formation of a dimer changes the energy of the system due to replacing two bonds of impurity with the host by one impurity-impurity bond. This assumes that the adatoms in dimeric state still remain in the substitutional positions. However, the molecular-dynamics calculation shows that this last assumption is not valid. In dimers, the Fe-Fe distances are shorter than the Ag-Ag nearest distances. This means some weakening of the remaining $2(Z-1)=22$ Fe-Ag repulsive bonds and a further gain in energy when a dimer is formed.

In the case of Au implanted with Fe, the Miedema model predicts a bonding energy for Fe dimer equal to -48 meV, which implies a clustering of iron atoms. This seems to be the case only for the samples implanted with 10^{15} and 2×10^{15} ions/cm^2, where the dimer fractions were found to be higher than their statistical probability, which leads to average energy $E_2^* = -180$ meV. For the sample, implanted with 5×10^{15} ions/cm^2, the dimer fraction is the same as calculated from a binominal distribution, which suggests a 0 bonding energy for dimers. For higher doses, i.e., 10^{16} and 2×10^{16} ion/cm^2, an anticlustering tendency is observed. For these samples, due to the high concentration of impurity atoms, the Eq. (5) may not be used for the determination of the dimer bonding energy. It should be noted that a considerable controversy regarding the clustering tendency of Fe in Au exists in the literature. For example, the enhanced clustering of Fe in implanted Au samples[7] or in as-rolled Fe-Au quenched alloys[26] was reported. However, in the recent work of Yoshida *et al.*[18] on diluted Fe-Au alloys studied by Mössbauer spectroscopy at high temperatures, i.e., on samples in thermodynamic equilibrium state, an anticlustering tendency was concluded. This was based on the negative short-range-order (SRO) parameter, α, defined as $\alpha=(n-c)/(1-c)$, where n is an average concentration of iron atoms in the nearest-neighbor shell, and c is the concentration of iron atoms in the whole sample. Since α was found to be temperature independent instead of increasing up to 0 in the high-temperature limit, higher-order correlation of Fe atoms in form of third-neighbor Fe-Fe pairs has been postulated.[18] This idea may be a key for solving the controversy as follows: in samples at thermodynamical equilibrium, the high-order correlation reduces the SRO parameter, while in very diluted quenched samples or in implanted specimens, such correlations are rather excluded; as a result, the iron aggregates are relatively more probable. Thus, it may be concluded that the Miedema approach is not exactly valid for the description of Fe-Au system. The calculated heats of solution are obtained by consideration of impurity atom immersed in the matrix host. For such a hypothetical situation formation of a dimer may lower the energy of the system compared with two isolated, not interacting atoms. However, in this way, only the local energy minimum of the system is achieved. A further energy gain is due to some high-order correlation of Fe

atoms.

It appears interesting to include in the discussion the data of Cu implanted with Fe.[10–12,14] All the authors report a very strong tendency for iron aggregation in this matrix. From the compilation of these data, one may estimate that in this case Fe-Fe bonding energy is of the order of −400 meV, which is much more than the value implied from corresponding heat of solutions (−92 meV).[1] However, in this case, the assumption of the melting temperature as the equilibrium temperature may not be adequate, because of the abnormally fast, enhanced by radiation damage, diffusion of Fe implanted in Cu. From the depth selective conversion electron Mössbauer spectra, it was found[15] that iron atoms are mobile even at 100 °C. Thus, the observed fraction of iron aggregates in Cu corresponds to an equilibrium temperature, which may be much lower than the melting temperature. Accordingly, the bonding energy may be significantly smaller than our estimate [cf. Eq. (5)] and closer to the Miedema model predictions.

(ii) State of iron implants in Ir, Pt, Rh and Ti. Due to the expected positive bonding energies (55, 82, 35, 107 meV for Ir, Pt, Rh, and Ti, respectively), which means repulsive interactions for iron impurities in these hosts, a strong predominance of the substitutional fraction is expected. For example, for a typical dimer energy of +80 meV, an iron concentration of 2%, and a temperature of 2000 °C the dimer fraction should be about 12% in comparison with 19% expected from a binomial distribution. Such dimer fraction, increasing with the dose, should be easily found in Mössbauer spectra. The experimental results contradict these predictions as discussed below.

The spectrum of Ir implanted with iron shows only substitutional iron ions in surroundings of cubic symmetry. An assignment of this iron state to iron monomers, even including experimental accuracy, leads to an unrealistic repulsive Fe-Fe potential of more than 400 meV. In the case of Pt the substitutional fraction, which may be assigned to the states with vanishing quadrupole interaction is about 93%, independent of the dose. In Rh the substitutional fraction is only about 40%, again, dose independent. The remaining iron states of strongly perturbed local symmetry cannot be identified as iron aggregates according to the following argumentation. The large amount of these aggregates would suggest an attractive potential between Fe-Fe atoms, being especially strong in Rh case in disagreement with the Miedema model prediction. On the other hand these states, in contrast to Ag, Au, and Cu cases, are unstable at moderate temperature, decomposing themselves into monomers, which is possible only for a repulsive potential. In addition, the *s*-electron density on ^{57}Fe nuclei in these states are lower than in the corresponding substitutional sites, again on the contrary to Ag, Au, and Cu cases, where the IS of Fe aggregates are less than IS of monomers, which is an evidence for an increase in *s*-electron density during clustering. Moreover, the fraction of these states is in both cases, Pt and Rh, dose independent, in contrast to the expected increase of Fe aggregates concentration with increasing dose. The last observation, i.e., the dose independence of the monomer fraction suggests that the Fe states exhibiting quadrupole interactions should be assigned to Fe atoms associated with structural defects. Indeed, for the dose range applied here, the concentration of defects is saturated. Thus, the probability for a Fe atom to be caught by a defect is constant, i.e., dose independent, as it is equal to $1-f_m$, where f_m is the monomer fraction. The geometry of Fe-defect aggregation may show a variety of configurations, which leads to a distribution of the hyperfine parameters, such as quadrupole splittings in the Pt case, or it may also be rather well determined giving discrete values for the corresponding IS or QS as in the Rh case. Such aggregates are not stable at sufficiently elevated temperatures. During annealing, Fe adatoms enter a substitutional position. It is interesting to note that even at quite high iron concentration in these matrices, when certainly some impurity atoms are located in the nearest-neighbor shell, only small distributions of quadrupole splitting are observed with unchanged isomer shifts. This may be explained as due to a positive potential of such iron aggregates excluding the bonding between them. As a result, up to certain concentrations of dopants there is no electron charge transfer between iron atoms and, consequently, the electron density at each ^{57}Fe nucleus is the same, independently on the local configuration of its first coordination shell.

The increase of IS (i.e., decrease of the *s*-electron density) of Fe embedded in complex with defects when compared with IS of Fe in substitutional sites is explained by the increase of the iron atomic volume. It is known from high-pressure Mössbauer experiments that IS in metals decreases with pressure in accordance with $d(\mathrm{IS})/d(V/V_0)=1.50(5)$ mm/s.[27] Thus, the increase of IS by 0.3–0.5 mm/s, as in the Rh case, may be related to the increase of iron atomic volume by 20–30 %. This argumentation points out dislocation loops and grain boundaries as possible traps for iron implants, at least for the Rh case. Accordingly, these defects which produce electric-field gradient at Fe sites without changing the IS may be related to imperfections of the host which are separated from Fe atoms.

In Ti, the Fe-Fe repulsive interactions are expected to be the strongest among the studied matrices. Therefore, the strong tendency for ordering is expected and, indeed, the Fe-Ti phase diagram is very complicated. For example, Stupel, Ron, and Weiss[20] reported six phases only in the titanium-rich (Fe contents <5 wt. %) Fe-Ti system. In the implanted samples, except Fe, in substitutional sites [hcp α-Ti(Fe) phase], an additional iron state, recognized as bcc β-Ti(Fe) phase was found. It means that in this system, the ordering process is fast enough to rearrange the local surrounding of iron during thermal spike.

CONCLUSIONS

Implanted iron impurities in the studied transition metals exhibit a lot of different local atomic arrangements. Although each host shows, in principle, its own peculiarity, some general hints for the approximate description of these complicated systems may be proposed as follows. The heats of solution of iron in transi-

tion metals are primary parameters determining the state of the corresponding implanted metastable systems.

For an attractive Fe-Fe potential, the requirement for the minimum of free energy leads to the formation of energetically favored iron aggregates. The relative ratio of these fractions, corresponding to a minimization of the free energy of the system, is determined by the related heats of solutions. It can be experimentally estimated from the distinct hyperfine interaction parameters assigned to each type of aggregate. The evaluation of the bonding energies of clusters is, however, strongly influenced by the uncertainty in the equilibrium temperature assigned to the system and by neglecting higher-order correlation of iron atoms. The defects formed during implantation, if not annealed, produce stable configurations which, being separated from iron impurities, have little influence on ^{57}Fe hyperfine parameters.

For a repulsive Fe-Fe potential, the iron monomers must be certainly a well-populated fraction. However, in this case the neighboring Fe atoms are not bonded and cannot be distinguished from isolated Fe atoms, jointly contributing to the substitutional line in the Mössbauer spectrum. Usually no ordering of Fe atoms is observed, at least for as-implanted samples, but a local minimum in the free energy is attainable during thermal spike, by trapping of the Fe implants by aggregates of defects. For very high Fe-Fe repulsive interaction, as in the Ti case, the local geometry of the host atoms surrounding iron impurity may be modified.

ACKNOWLEDGMENTS

The work was supported by IN2P3 program (Project No. 52) and by Polish Grant No. 201039101.

[1]F. R. de Boer, R. Boom, W. C. M. Mattens, A. R. Miedema, and A. K. Niessen, *Cohesion in Metals, Transition Metal Alloys* (North-Holland, Amsterdam, 1988).

[2]A. Z. Hrynkiewicz and K. Krolas, Phys. Rev. B **28**, 1864 (1983).

[3]K. Krolas, Phys. Lett. **85A**, 107 (1981).

[4]K. Krolas, Z. Inglot, and M. Sternik, in *Proceedings of the XXIV Zakopane School on Physics, Zakopane 1989,* edited by J. Stanek and A. Pedziwiatr (World Scientific, Singapore, 1989), p. 3.

[5]B. D. Sawicka, Nucl. Instrum. Methods Phys. Res. **182/183**, 1039 (1981).

[6]B. D. Sawicka and J. A. Sawicki in *The Exotic Side of the Method,* edited by U. Gonser, Topics in Current Physics Vol. 25 (Springer Verlag, Berlin, 1981), p. 139.

[7]B. D. Sawicka and J. A. Sawicki, Nucl. Instrum. Methods Phys. Res. **209/210**, 799 (1983).

[8]G. Marest, H. Jaffrezic, J. Stanek, and H. Binczycka, Nucl. Instrum. Methods Phys. Res. Sect. B **80/81**, 357 (1993).

[9]G. Longworth and R. Jain, J. Phys. F **8**, 993 (1978).

[10]G. Longworth and R. Jain, J. Phys. (Paris) Colloq. **40**, C2-608 (1979).

[11]B. D. Sawicka, J. A. Sawicki, and J. Stanek, Phys. Lett. **59A**, 59 (1976).

[12]B. D. Sawicka and J. A. Sawicki, J. Phys. (Paris) Colloq. **40**, C2-576 (1979).

[13]D. C. Khan and N. V. Nair, Hyperfine Interact. **28**, 1001 (1986).

[14]B. Window, Philos. Mag. **26**, 681 (1972).

[15]H. Anderson, S. Damgaard, J. W. Petersen, and G. Weyer, Hyperfine Interact. **15/16**, 335 (1983).

[16]J. F. Ziegler, J. P. Biersack, and U. Littmark, *The Stopping and Range of Ions in Solids* (Pergamon, New York, 1985), Vol. 1.

[17]G. Le Caer and J. M. Dubois, J. Phys. E **12**, 1983 (1979).

[18]Y. Yoshida, F. Langmay, P. Fratzl, and G. Vogl, Phys. Rev. B **39**, 6395 (1989).

[19]K. Sumiyama, H. Ezawa, and Y. Nakamura, Phys. Status Solidi A **493**, 81 (1986).

[20]M. M. Stupel, M. Ron, and B. Z. Weiss, J. Appl. Phys. **447**, 6 (1976).

[21]M. P. Allen and D. J. Tildeslay, *Computer Simulation of Liquids* (Oxford University, New York, 1987).

[22]V. Rosato, M. Guillope, and B. Legrand, Philos. Mag. **59**, 321 (1989).

[23]M. Guillope and B. Legrand, Surf. Sci. **215**, 577 (1989).

[24]H. J. Berendsen, J. P. M. Postma, and W. R. Haak, J. Chem. Phys. **81**, 3684 (1984).

[25]L. Verlet, Phys. Rev. **159**, 98 (1967).

[26]G. L. Whittle and S. J. Campbell, J. Phys. F **15**, 693 (1985).

[27]T. C. Gibb and N. N. Greenwood, *Mössbauer Spectroscopy* (Chapman and Hall, London, 1971), p. 307.